Extreme erosion by submarine slides

Harya D. Nugraha[1,2]*, Christopher A.-L. Jackson[2,3], Howard D. Johnson[2], David M. Hodgson[4] and Michael A. Clare[5]

[1]Center for Sustainable Geoscience (CSG), Universitas Pertamina, Jakarta 12220, Indonesia
[2]Basins Research Group (BRG), Imperial College, London SW7 2BP, UK
[3]Department of Earth and Environmental Sciences, University of Manchester, Manchester M13 9PL, UK
[4]School of Earth and Environment, University of Leeds, Leeds LS2 9JT, UK
[5]Ocean BioGeoscience, National Oceanography Centre, Southampton SO14 3ZH, UK

ABSTRACT

Submarine slides (including slides, slumps, and debris flows) pose major geohazards by triggering tsunami and damaging essential submarine infrastructure. Slide volume, a key parameter in hazard assessments, can increase markedly through substrate and/or water entrainment. However, the erosive potential of slides is uncertain. We quantified slide erosivity by determining the ratio of deposited (V_d) to initially evacuated (V_e) sediment volumes; i.e., slides that gain volume through erosion have a V_d/V_e ratio >1. We applied this method to the Gorgon slide, a large (500 km³), seismically imaged slide offshore northwestern Australia, and reviewed V_d/V_e ratios for 11 other large slides worldwide. Nine of the 11 slides have V_d/V_e > 1 (median value = 2), showing emplaced volumes increased after initial failure. The Gorgon slide is the most erosive slide currently documented (V_d/V_e = 13), possibly reflecting its passage across a highly erodible carbonate ooze substrate. Our new approach to quantifying erosion is important for hazard assessments given substrate-flow interactions control slide speed and runout distance. The variations in slide volume also have important implications for submarine infrastructure impact assessments, including more robust tsunami modeling.

INTRODUCTION

Submarine slope failure results in a range of mass-flow types including slides, slumps, debris flows, and their transitions. It is a key process along many continental margins, with individual deposit volumes sometimes exceeding 10,000 km³ (e.g., Moscardelli and Wood, 2016). Mass flows can be tsunamigenic and deadly (Tappin et al., 2001) and damage vital seabed infrastructure, such as telecommunication cables (Carter et al., 2014) and hydrocarbon pipelines (e.g., Randolph and White, 2012). Most studies have focused on the size and impact of slope failure of siliciclastic sediment (e.g., ten Brink et al., 2006; Moscardelli and Wood, 2016), despite carbonate ooze composing a significant portion (~30%) of the world's ocean floor (see Fig. S1 in the Supplemental Material[1]; Dutkiewicz et al., 2015). Post-failure shear strength of such oozes can be as low as 10% of its original strength, compared to 55% for siliciclastic clay (Gaudin and White, 2009), allowing ooze-related mass flows to gain volume during transport more easily and become more hazardous (Winterwerp et al., 2012).

A mass flow may translate across its substrate on a thin, highly pressured, basal water layer ("hydroplaning"; e.g., Mohrig et al., 1998; Toniolo et al., 2004) and may even suffer volume loss due to partial flow transformation from debris flow to turbidity current (e.g., Sun et al., 2018). However, mass flows can be strongly erosive (e.g., Bull et al., 2009; Hodgson et al., 2018; Sobiesiak et al., 2018), although the magnitude of substrate entrainment is poorly constrained due to limited exposure of exhumed deposits and their source areas and poor or spatially restricted imaging in subsurface data. Quantifying mass-flow erosivity is important because (1) entrainment of material during transport via basal erosion could modify flow rheology, speed, and runout distance, the latter two being key parameters for both tsunami modeling and impact assessments on submarine infrastructure (e.g., Bruschi et al., 2006); and (2) initial failed volume is a key parameter in tsunami modeling (e.g., Murty, 2003).

We used three-dimensional (3-D) seismic reflection data from the Exmouth Plateau, offshore northwestern Australia, to quantify erosion by the Gorgon slide (Fig. 1). We focused on the discrepancy between the volume of evacuated (V_e) and deposited (V_d) sediment to provide a first-order estimate of slide erosivity. We also documented V_d and V_e for 11 other examples. Our approach (1) provides insights into the likely physical processes occurring during slide transport; (2) improves prediction of the impact of slope failure on submarine infrastructure; and (3) better constrains numerical models of slide-induced tsunami.

GEOLOGICAL SETTING

The Cenozoic sedimentary history of the Exmouth Plateau (Fig. 1A) is dominated by carbonate ooze deposition (Longley et al., 2002), with repeated slope failure and mass-flow emplacement triggered by intraplate shortening and folding (Keep et al., 1998) and related seismicity (see Hengesh et al. [2013] for detailed geological setting). Here we focus on the most recent and shallowly buried, and thus best-imaged, example, the Gorgon slide (Figs. 1B and 1C).

DATASET AND METHODS

Five time-migrated 3-D seismic reflection data sets (Fig. 1; see also Table S1 in the Supplemental Material) image the Gorgon slide, its source area, and the adjacent, unfailed continental slope (Figs. 1B and 1C). A near-seabed sediment seismic velocity of 1824 m/s and dominant seismic frequency of 40–60 Hz indicate the vertical seismic resolution at the base of the Gorgon slide (~500 m below seabed) is 8–11 m. We depth-converted maps of the top and base of the Gorgon slide (see Figs. 1D and 1E) using

*E-mail: harya.dn@universitaspertamina.ac.id
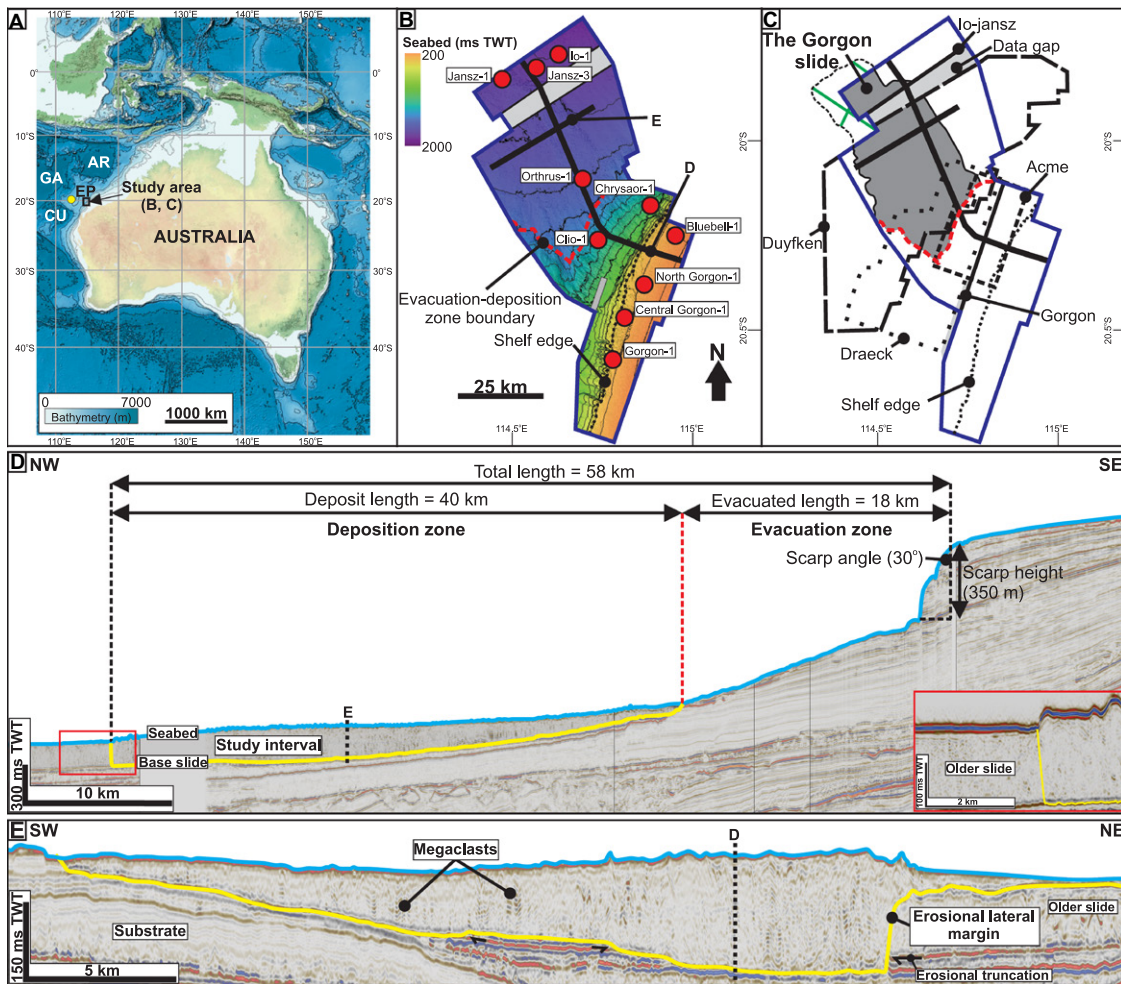
Figure 1. (A) Location of the study area in northwestern Australia (EP—Exmouth Plateau; AR—Argo Abyssal Plain; GA—Gascoyne Abyssal Plain; CU—Cuvier Abyssal Plain). Yellow dot is Ocean Drilling Program Site 762 well. (B) Seabed map (top of Gorgon slide) showing slide evacuation and deposition zones. Red dots are wells used for depth conversion. TWT—two-way traveltime. (C) Extent of the Gorgon slide (gray). Black dashed line in the northernmost part of the slide defines the seismic-scale pinchout of the slide; ~7% of the slide is outside the three-dimensional (3-D) seismic data but is mapped on two-dimensional seismic profiles (green lines). Gorgon, Acme, Draeck, Duyfken, and Io-jansz are Geoscience Australia 3-D seismic data sets used in this study (see Table S1 [see footnote 1]). (D) Northwest-trending depositional dip–oriented seismic profile across the Gorgon slide, showing evacuation and deposition zones. Inset seismic section (red outline) shows frontal geometry of the Gorgon slide. (E) Northeast-trending depositional strike seismic profile across the Gorgon slide (note truncation at slide base).

average water (1519 m/s) and near-seabed sediment (1824 m/s) seismic velocities, respectively (Table S1). Ten wells constrain the water seismic velocity (Fig. 1B). Ocean Drilling Program (ODP) Site 762 (see Fig. 1A) penetrates a seismic-stratigraphic sequence similar to that of the study area. We therefore used data from this well to infer near-seabed seismic velocity (see above) and lithology and porosity.

We calculated the ratio between V_e and V_d to derive a first-order estimate of slide erosivity (Fig. S2A). When $V_d/V_e < 1$, we infer the slide lost volume during transport; this could reflect water loss and partial flow transformation to turbidity currents that deposited basinward (Fig. S2B). $V_d/V_e = 1$ suggests no net volume change from the initial failed mass (e.g., entrained sediment volume balanced by volume loss due to flow transformation) (Fig. S2C). $V_d/V_e > 1$ implies net volume gain during transport due to lengthening and/or deepening (by erosion) of the basal-shear surface and substrate entrainment (Fig. S2D).

We calculated the V_d/V_e ratio for the Gorgon slide using three established methods to capture volume uncertainty (see Table S2 for details): (1) theoretical volume (e.g., McAdoo et al., 2000; Wilson et al., 2004); (2) bulk volume (e.g., Piper et al., 1997); and (3) compacted volume (assuming theoretical zero porosity) (e.g., Lamarche et al., 2008).

EROSIVITY OF SUBMARINE SLIDES
The Gorgon Slide

The updip margin of the Gorgon slide source area is defined by a steep headscarp. The parent flow traveled ~70 km northwestward from its evacuation zone before accumulating sediment in a depositional zone (Fig. 1D). The slide was confined downdip by its frontal toewall (i.e., frontally confined; *sensu* Frey-Martínez et al., 2006). The slide deposit is ~30 km wide, thickens downslope to ~500 m, and covers a total area of 1760 km². Transparent, chaotic seismic reflections support interpretation of a debrite (Figs. 1D and 1E) (e.g., Posamentier and Martinsen, 2011). Discrete packages of subparallel, high-amplitude reflections are likely megaclasts (Fig. 1E) (e.g., Jackson, 2011), either sourced from the evacuation zone or entrained from the substrate. Key evidence of basal erosion is the truncation of underlying reflections (Fig. 1E).

We calculated the V_d of the Gorgon slide using the basal-shear surface and seabed (see Figs. 1D and 1E). This represents a minimum value, given a very small part (~7%; i.e., 166 km² of 1760 km²; see Fig. 1C) of the slide is not imaged within the seismic data set. The headscarp of the slide extends from a lateral scarp in the southwest to a gullied slope in the northeast (Figs. 2A–2C). The headscarp may extend further northeast outside of the area of the available data set, given a lateral scarp is not confidently identified there (such as in Fig. 2B). However, we argue any lateral scarp is unlikely to lie beyond the seismically imaged area given that we can trace numerous basal grooves (see Bull et al., 2009) updip from the deposit to the source area and bounding headscarp. The deposit's northeastern lateral margin also connects directly back to its source area, suggesting the northeastern limit of the headscarp (and thus evacuation zone) lies very close to the gullied slope (Figs. 2A and 2C) (see also Hengesh et al., 2013, their figure 8). To reflect this uncertainty, our V_e estimates comprise minimum (Fig. 2A) and maximum (Fig. 2D) cases (see Fig. S3). Note that V_e was estimated by using the adjacent unfailed slope as a proxy for the pre-failure physiography across the evacuation zone
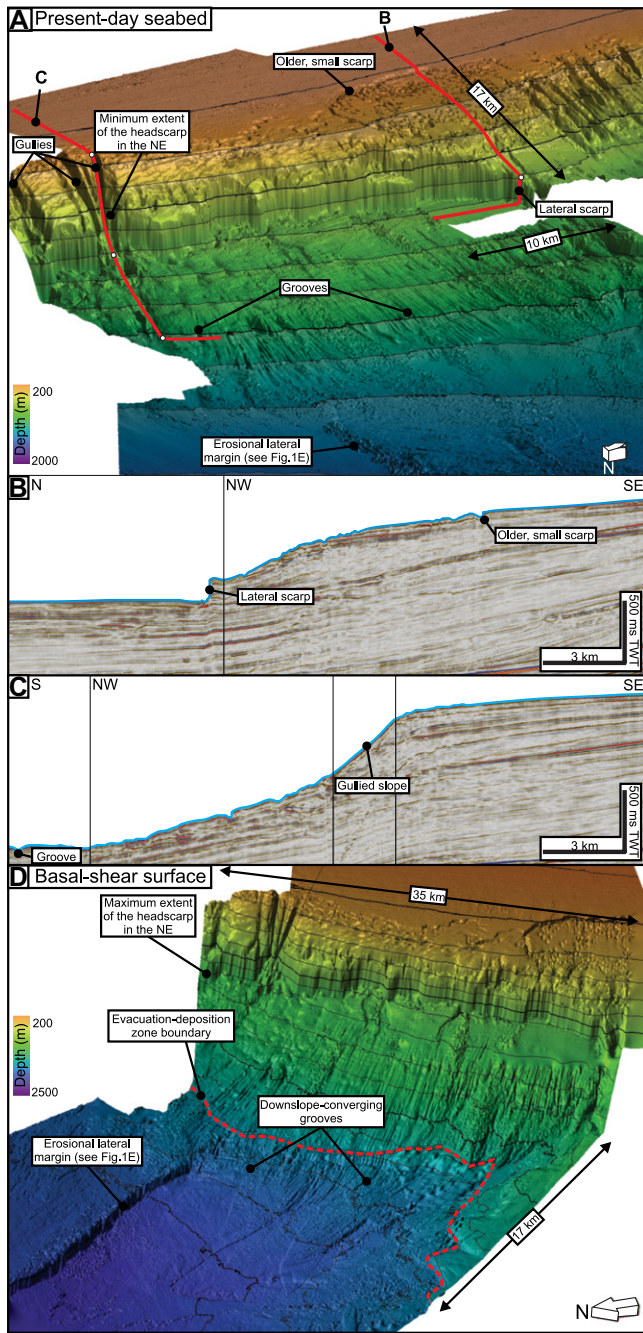
Figure 2. (A) Three-dimensional (3-D) perspective of the seabed at the Gorgon slide (northwestern Australia) showing lateral scarp in the southwest and minimum extent of the headscarp marked by the presence of a gullied slope. Grooves that can be traced back from the deposit to the source are also shown. (B) Seismic profile across the lateral scarp limiting the headscarp in the southwest. (C) Seismic profile across a gully that may define the northeastern limit of the headscarp. TWT—two-way traveltime. (D) 3-D perspective of basal-shear surface showing downslope-converging grooves that indicate that parent flow was focused to the northeast and thus formed a straight, erosional lateral margin.
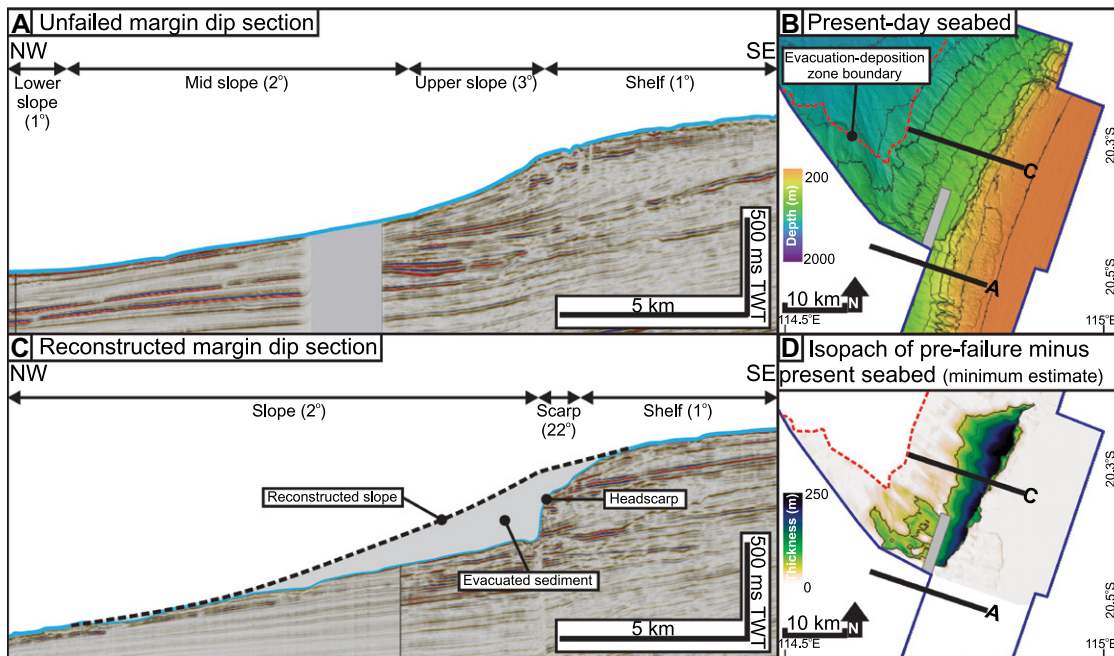
tion zone was enlarged by post-failure tectonics) (Collot et al., 2001).

DISCUSSION
Large Submarine Slides are Predominantly Erosive

We show that deposit volumes of submarine slides are typically larger than their initial failed volumes, thereby confirming the erosivity of their parent mass flows. Substrate entrainment and volume gain occurs when the shear stress exerted by an overriding flow exceeds the shear strength of its substrate. The overriding flow may also elevate substrate pore pressures, reducing substrate strength and making it more susceptible to entrainment. Substrate entrainment can also occur due to "tooling" by rigid blocks (e.g., megaclasts; Hodgson et al. 2018). Our study thus supports physical experiments, which suggest that relatively dense debris flows can load, shear, and entrain their substrate and thus increase in volume (Toniolo et al., 2004). The mechanistic causes controlling the magnitude of erosion at the base of mass flows remain unknown. Toniolo et al. (2004) provided experimental evidence and an analytical argument suggesting that the loading-related component of erosion reflects antecedent deposit density, yield strength, thickness, and seabed slope angle (which together control the resistance of the substrate to shear exerted by the overriding flow), whereas seabed rugosity controls the degree of shear-related erosion (which controls the substrate shearing by the overriding slide).

To assess the Toniolo et al. (2004) predictions, we plotted several commonly measured slide parameters (i.e., evacuated volume, runout distance, height drop, and mobility; for terminology, see Hampton et al., 1996) to investigate their potential relationship with slide erosivity (see Fig. S4). We found no significant relationship between these parameters ($R^2 = 0.0002$–0.05), suggesting low predictive power and that other factors are at play. For example, an abrupt decrease in slope gradient may increase the vertical impact of the slide on the substrate, resulting in more erosion (Ogata et al., 2014; see also Sammartini et al. 2021). Likewise, the pre-failure substrate morphology and composition may be important controls on slide erosivity, given these may, respectively, focus the parent flow and determine spatial patterns of erosion (e.g., a clay-rich substrate is typically more resistant to erosion than a clay-poor substrate due to electrochemical forces between particles; Ortiz-Karpf et al., 2017). In the case of the Gorgon slide, we note that the basal shear surface broadly follows underlying substrate morphology (Fig. 1E) and contains downslope-converging grooves (Fig. 2D). These observations imply that the parent flow was focused on the northeastern side of the slide, resulting in a straight, erosional lateral margin (see Figs. 1E and 2D).
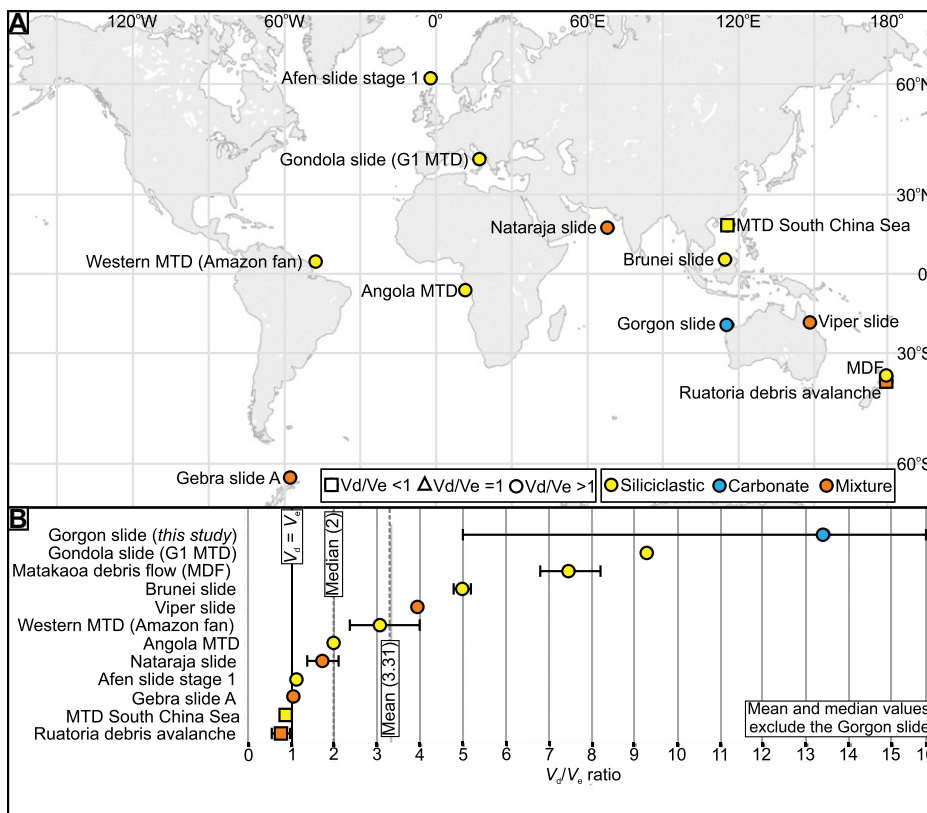
(Fig. 3). Our analysis shows that the estimated V_d/V_e ratio for the Gorgon slide ranges from 5 to 16, depending on the calculation method used and taking into account uncertainties related to the position of the headscarp and lateral margin and thus the total evacuation zone volume (see Fig. S3). The entire range of calculations, accounting for the full range of uncertainty, suggests the slide was strongly erosive (i.e., $V_d/V_e > 1$), a result consistent with the abundant evidence for seismic-scale erosion along the basal-shear surface (Fig. 3B).

Global Analysis of Slide Erosivity

To place our results in a global context, we collated data from other slides (see Table S3).

Of the 357 slides documented in 97 studies, only 11 presented both V_e and V_d, with 9 of these 11 slides being erosive ($V_d/V_e > 1$, with a median value of 2 and an average value of 3; Fig. 4). The Gorgon slide ($V_d/V_e = 5$–16) is thus the most erosive slide yet documented (Fig. 4B). Although most are erosive, two slides have $V_d/V_e < 1$ (Fig. 4B): (1) in the South China Sea, where volume loss is attributed to partial flow transformation from mass flow to turbidity current, resulting in (sub-seismic-resolution) turbidites, and pore-volume reduction due to continuous shearing during transport (Sun et al., 2018); and (2) in New Zealand, where the evacuation zone formed due to slope failure and tectonic erosion during seamount subduction (i.e., the evacua-

Figure 3. (A) Northwest-trending seismic profile across the unfailed margin. (B) Seabed depth-structure map showing the headscarp of the Gorgon slide (northwestern Australia) and the adjacent unfailed margin to the southwest. TWT—two-way traveltime. (C) Northwest-trending seismic profile across the headscarp of the Gorgon slide and reconstructed (i.e., pre-failure) seabed. (D) Isopach of difference between reconstructed pre-failure seabed and depth-structure map, assuming minimum extent of the headscarp.

The Gorgon slide and other ooze-dominated slides may be especially erosive because their substrates were dominated by fragile foraminifera and nannofossils, which are only weakly cemented at their contacts during early burial. This preserves unusually high near-surface porosities and results in higher initial strength than in (uncemented) siliciclastic sediments (O'Brien and Manghnani, 1992). Under loading, these fragile biogenic particles are crushed, which generates excess near-seabed pore pressures and a dramatic loss of strength (e.g., Sharma and Joer, 2015). When carbonate oozes fail, their residual strength can be only 10% of their initial strength, compared to as much as 55% for siliciclastic sediment (see Fig. S5; Gaudin and White, 2009).

Implications of Submarine Slide Erosivity for Geohazard Assessments

The V_d/V_e ratio provides a first-order, quantitative estimate of whether a slide increases or decreases its volume during transport, which mainly depends on processes at the base of mass flows. When a slide is erosive and "bulks up", it may (1) slow down due to enhanced basal friction, thereby reducing runout distance (e.g., Schulz et al., 2009), or (2) speed up due to the added mass, thereby increasing runout distance (e.g., Gee et al., 1999). Conversely, when a slide hydroplanes and does not erode its substrate, both its transport speed and runout distance may increase (e.g., Mohrig et al., 1998). Slide speed and runout distance are key components for tsunami modeling (e.g., Murty, 2003) and for assessing the potential impact slides may have on submarine infrastructure (e.g., Bruschi et al., 2006). In addition, V_e is also a key factor for tsunami modeling because it dictates how much overlying water is displaced during failure (e.g., Murty, 2003). Accurate volume assessment is especially challenging if only V_d is known and if there is significant erosion or partial flow transformation. For example, the use of V_d as an estimate of V_e for tsunami modeling would overestimate displacement of the overlying water when $V_d/V_e > 1$. Conversely, if $V_d/V_e < 1$, tsunami modeling would underestimate the displacement of the overlying water.

Figure 4. (A) World distribution of documented slides in peer-reviewed literature, containing information on evacuated (V_e) and deposited (V_d) volumes. Note that the Gorgon slide (northwestern Australia) is the only carbonate-dominated slide. MTD—mass-transport deposit. (B) V_d/V_e ratio of submarine slides in A. Error bars represent minimum and maximum values obtained from different volume calculation methods. References for each slide are available in Table S3 (see footnote 1).

Therefore, to understand uncertainties associated with tsunami modeling, a range of V_d/V_e scenarios should be considered. Our study suggests that most slides are erosive and that a ratio of 1 to at least 2 (median value) should be used for scenario modeling. Carbonate ooze–dominated slides such as the Gorgon slide, which have only rarely been documented to date, could also be significantly more erosive than siliciclastic slides.

REFERENCES CITED
Bruschi, R., Bughi, S., Spinazzè, M., Torselletti, E., and Vitali, L., 2006, Impact of debris flows and turbidity currents on seafloor structures: Norwegian Journal of Geology (Norsk Geologisk Forening), v. 86, no. 3, p. 317–337.

Bull, S., Cartwright, J., and Huuse, M., 2009, A review of kinematic indicators from mass-transport complexes using 3D seismic data: Marine and Petroleum Geology, v. 26, p. 1132–1151, https://doi.org/10.1016/j.marpetgeo.2008.09.011.

Carter, L., Gavey, R., Talling, P.J., and Liu, J.T., 2014, Insights into submarine geohazards from breaks in subsea telecommunication cables: Oceanography (Washington, D.C.), v. 27, p. 58–67, https://doi.org/10.5670/oceanog.2014.40.

Collot, J.Y., Lewis, K., Lamarche, G., and Lallemand, S., 2001, The giant Ruatoria debris avalanche on the northern Hikurangi margin, New Zealand: Result of oblique seamount subduction: Journal of Geophysical Research: Solid Earth, v. 106, B9, p. 19,271–19,297, https://doi.org/10.1029/2001JB900004.

Dutkiewicz, A., Müller, R.D., O'Callaghan, S., and Jónasson, H., 2015, Census of seafloor sediments in the world's ocean: Geology, v. 43, p. 795–798, https://doi.org/10.1130/G36883.1.

Frey-Martínez, J., Cartwright, J., and James, D., 2006, Frontally confined versus frontally emergent submarine landslides: A 3D seismic characterisation: Marine and Petroleum Geology, v. 23, p. 585–604, https://doi.org/10.1016/j.marpetgeo.2006.04.002.

Gaudin, C., and White, D.J., 2009, New centrifuge modelling techniques for investigating seabed pipeline behaviour, in Hamza, M., et al., eds., Proceedings of the 17th International Conference on Soil Mechanics and Geotechnical Engineering, 5–9 October 2009, Alexandria, Egypt: Amsterdam, IOS Press, p. 448–451, https://doi.org/10.3233/978-1-60750-031-5-448.

Gee, M.J.R., Masson, D.G., Watts, A.B., and Allen, P.A., 1999, The Saharan debris flow: An insight into the mechanics of long runout submarine debris flows: Sedimentology, v. 46, p. 317–335, https://doi.org/10.1046/j.1365-3091.1999.00215.x.

Hampton, M.A., Lee, H.J., and Locat, J., 1996, Submarine landslides: Reviews of Geophysics, v. 34, p. 33–59, https://doi.org/10.1029/95RG03287.

Hengesh, J.V., Dirstein, J.K., and Stanley, A.J., 2013, Landslide geomorphology along the Exmouth Plateau continental margin, North West Shelf, Australia: Australian Geomechanics, v. 48, p. 71–92.

Hodgson, D.M., Brooks, H.L., Ortiz-Karpf, A., Spychala, Y., Lee, D.R., and Jackson, C.A.-L., 2018, Entrainment and abrasion of megaclasts during submarine landsliding and their impact on flow behaviour, in Lintern, D.G., et al., eds., Subaqueous Mass Movements and their Consequences: Assessing Geohazards, Environmental Implications and Economic Significance of Subaqueous Landslide: Geological Society, London, Special Publication 477, p. 223–240, https://doi.org/10.1144/SP477.26.

Jackson, C.A.-L., 2011, Three-dimensional seismic analysis of megaclast deformation within a mass transport deposit: Implications for debris flow kinematics: Geology, v. 39, p. 203–206, https://doi.org/10.1130/G31767.1.

Keep, M., Powell, C.M., and Baillie, P.W., 1998, Neogene deformation of the North West Shelf, Australia, in Purcell, P.G., and Purcell, R.R., eds., The Sedimentary Basins of Western Australia 2: Perth, Petroleum Exploration Society of Australia, Western Australian Branch, p. 81–91.

Lamarche, G., Joanne, C., and Collot, J.-Y., 2008, Successive, large mass-transport deposits in the south Kermadec fore-arc basin, New Zealand: The Matakaoa Submarine Instability Complex: Geochemistry Geophysics Geosystems, v. 9, Q04001, https://doi.org/10.1029/2007GC001843.

Longley, I.M., et al., 2002, The North West Shelf of Australia—A Woodside perspective, in Keep, M., and Moss, S.J., eds., The Sedimentary Basins of Western Australia 3: Perth, Petroleum Exploration Society of Australia, p. 28–88.

McAdoo, B.G., Pratson, L.F., and Orange, D.L., 2000, Submarine landslide geomorphology, US continental slope: Marine Geology, v. 169, p. 103–136, https://doi.org/10.1016/S0025-3227(00)00050-5.

Mohrig, D., Ellis, C., Parker, G., Whipple, K.X., and Hondzo, M., 1998, Hydroplaning of subaqueous debris flows: Geological Society of America Bulletin, v. 110, p. 387–394, https://doi.org/10.1130/0016-7606(1998)110<0387:HOSDF>2.3.CO;2.

Moscardelli, L., and Wood, L., 2016, Morphometry of mass-transport deposits as a predictive tool: Geological Society of America Bulletin, v. 128, p. 47–80, https://doi.org/10.1130/B31221.1.

Murty, T.S., 2003, Tsunami wave height dependence on landslide volume: Pure and Applied Geophysics, v. 160, p. 2147–2153, https://doi.org/10.1007/s00024-003-2423-z.

O'Brien, D.K., and Manghnani, M.H., 1992, Physical properties of Site 762: A comparison of shipboard and shore-based laboratory results, in von Rad, U., et al., eds., Proceedings of the Ocean Drilling Program, Scientific Results, Volume 122: College Station, Texas, Ocean Drilling Program, p. 349–362.

Ogata, K., Pogačnik, Ž., Pini, G.A., Tunis, G., Festa, A., Camerlenghi, A., and Rebesco, M., 2014, The carbonate mass transport deposits of the Paleogene Friuli Basin (Italy/Slovenia): Internal anatomy and inferred genetic processes: Marine Geology, v. 356, p. 88–110, https://doi.org/10.1016/j.margeo.2014.06.014.

Ortiz-Karpf, A., Hodgson, D.M., Jackson, C.A.-L., and McCaffrey, W.D., 2017, Influence of seabed morphology and substrate composition on mass-transport flow processes and pathways: Insights from the Magdalena Fan, offshore Colombia: Journal of Sedimentary Research, v. 87, p. 189–209, https://doi.org/10.2110/jsr.2017.10.

Piper, D.J.W., Pirmez, C., Manley, P.L., Long, D., Flood, R.D., Normark, W.R., and Showers, W., 1997, Mass transport deposits of the Amazon Fan, in Flood, R.D., et al., eds., Proceedings of the Ocean Drilling Program, Scientific Results, Volume 155: College Station, Texas, Ocean Drilling Program, p. 109–146, https://doi.org/10.2973/odp.proc.sr.155.212.1997.

Posamentier, H.W., and Martinsen, O.J., 2011, The character and genesis of submarine mass-transport deposits: Insights from outcrop and 3D seismic data, in Shipp, R.C., et al., eds., Mass-Transport Deposits in Deepwater Settings: Society for Sedimentary Geology (SEPM) Special Publication 96, p. 7–38, https://doi.org/10.2110/sepmsp.096.007.

Randolph, M.F., and White, D.J., 2012, Interaction forces between pipelines and submarine slides—A geotechnical viewpoint: Ocean Engineering, v. 48, p. 32–37, https://doi.org/10.1016/j.oceaneng.2012.03.014.

Sammartini, M., Moernaut, J., Kopf, A., Stegmann, S., Fabbri, S.C., Anselmetti, F.S., and Strasser, M., 2021, Propagation of frontally confined subaqueous landslides: Insights from combining geophysical, sedimentological, and geotechnical analysis: Sedimentary Geology, v. 416, 105877, https://doi.org/10.1016/j.sedgeo.2021.105877.

Schulz, W.H., McKenna, J.P., Kibler, J.D., and Biavati, G., 2009, Relations between hydrology and velocity of a continuously moving landslide—Evidence of pore-pressure feedback regulating landslide motion?: Landslides, v. 6, p. 181–190, https://doi.org/10.1007/s10346-009-0157-4.

Sharma, S.S., and Joer, H.A., 2015, Some characteristics of carbonate sediments from North West Shelf, Western Australia, in Meyer, V., ed., Frontiers in Offshore Geotechnics III: Proceedings of the Third International Symposium on Frontiers in Offshore Geotechnics (ISFOG 2015), Oslo, Norway, 10–12 June 2015: London, CRC Press, v. 1, p. 1109–1114.

Sobiesiak, M.S., Kneller, B., Alsop, G.I., and Milana, J.P., 2018, Styles of basal interaction beneath mass transport deposits: Marine and Petroleum Geology, v. 98, p. 629–639, https://doi.org/10.1016/j.marpetgeo.2018.08.028.

Sun, Q.L., Alves, T.M., Lu, X.Y., Chen, C.X., and Xie, X.N., 2018, True volumes of slope failure estimated from a Quaternary mass-transport deposit in the northern South China Sea: Geophysical Research Letters, v. 45, p. 2642–2651, https://doi.org/10.1002/2017GL076484.

Tappin, D.R., Watts, P., McMurtry, G.M., Lafoy, Y., and Matsumoto, T., 2001, The Sissano, Papua New Guinea tsunami of July 1998—Offshore evidence on the source mechanism: Marine Geology, v. 175, p. 1–23, https://doi.org/10.1016/S0025-3227(01)00131-1.

ten Brink, U.S., Geist, E.L., and Andrews, B.D., 2006, Size distribution of submarine landslides and its implication to tsunami hazard in Puerto Rico: Geophysical Research Letters, v. 33, L11307, https://doi.org/10.1029/2006GL026125.

Toniolo, H., Harff, P., Marr, J., Paola, C., and Parker, G., 2004, Experiments on reworking by successive unconfined subaqueous and subaerial muddy debris flows: Journal of Hydraulic Engineering, v. 130, p. 38–48, https://doi.org/10.1061/(ASCE)0733-9429(2004)130:1(38).

Wilson, C.K., Long, D., and Bulat, J., 2004, The morphology, setting and processes of the Afen Slide: Marine Geology, v. 213, p. 149–167, https://doi.org/10.1016/j.margeo.2004.10.005.

Winterwerp, J.C., van Kesteren, W.G.M., van Prooijen, B., and Jacobs, W., 2012, A conceptual framework for shear flow–induced erosion of soft cohesive sediment beds: Journal of Geophysical Research, v. 117, C10020, https://doi.org/10.1029/2012JC008072.

Printed in USA